

Simultaneous ASCA And RXTE Observations of Cygnus X–1 During Its 1996 State Transition

Wei Cui¹, K. Ebisawa^{2,3}, T. Dotani⁴, and A. Kubota⁵

ABSTRACT

We report results from simultaneous ASCA and RXTE observations of Cygnus X–1 when the source made a rare transition from the hard (= low) state to the soft (= high) state in 1996. These observations together cover a broad energy range ~ 0.7 –50 keV with a moderate energy resolution at the iron K-band, thus make it possible to disentangle various spectral components. The low-energy spectrum is dominated by an ultra-soft component, which is likely to be the emission from the hottest inner portion of the accretion disk around the black hole. At high energies, the X-ray spectrum can be described by a Comptonized spectrum with a reflection component. The Compton corona, which upscatters soft “seed photons” to produce the hard X-ray emission, is found to have a y -parameter ~ 0.28 . The hard X-ray emission illuminates the accretion disk and the re-emitted photons produce the observed “reflection bump”. We show that the reflecting medium subtends only a small solid angle ($\sim 0.15 \times 2\pi$), but has a large ionization parameter such that iron is ionized up to Fe XXIV–Fe XXVI. The presence of a broad iron line at 6.58 ± 0.04 keV is also consistent with a highly ionized disk, if we take into account the gravitational and Doppler shift of the line energy. These results imply a geometry with a central corona surrounding the black hole and the reflection occurring in the innermost region of the disk where matter is highly ionized.

Subject headings: binaries: general — stars: individual (Cygnus X–1) — X-rays: stars

1. INTRODUCTION

Cygnus X–1 is considered as an archetypical stellar-mass black hole candidate (BHC). Its observed spectral and temporal X–ray properties have, therefore, often been used to distinguish

¹Center for Space Research, Massachusetts Institute of Technology, Cambridge, MA 02139

²code 660.2, NASA/GSFC, Greenbelt, MD 20771

³also Universities Space Research Association

⁴Institute of Space and Astronautical Science, Yoshinodai, Sagami-hara, Kanagawa, 229, Japan

⁵Department Physics, University of Tokyo, Hongo, Bunkyo-ku, Tokyo, 113 Japan

black hole binaries from their neutron star counterparts. Though seriously flawed, this approach has resulted in the discovery of many BHCs whose candidacy was later confirmed by dynamical mass determination based on optical observations. Despite such success, little is known about the physics behind many observed phenomena in Cyg X–1, such as its occasional state transitions and details of its hard X-ray production mechanism(s).

Much attention (Belloni et al. 1996; Cui et al. 1997a,b,c; Zhang et al. 1997; Dotani et al. 1997) has been paid to the recent transition of Cyg X–1 in 1996 from its usual hard (or low) state to the rare soft (or high) state discovered by the All-Sky Monitor (ASM) on *Rossi X-ray Timing Explorer* (RXTE) (Cui 1996), because no similar transitions had been seen since 1980 (Ogawara et al. 1982). This time, nearly continuous coverage of the transition were provided simultaneously by two complementary all-sky monitors: ASM/RXTE in the soft band (1.3–12 keV) and BATSE/CGRO in the hard band (20–200 keV) through the entire period. Not only was the anti-correlation (or “spectral pivoting”) between the soft and hard X-rays firmly established, but more surprisingly the bolometric X-ray luminosity varied little during the transition (Zhang et al. 1997). This is very different from X-ray outbursts observed in transient BHCs during which X-ray luminosity usually changes by more than an order of magnitude.

Snapshots were also taken during the transition and in the soft state with more sensitive instruments on several satellites including RXTE (Belloni et al. 1996; Cui et al. 1997a,b,c), ASCA (Dotani et al. 1997), and OSSE/CGRO. At high energies ($\gtrsim 10$ keV), the observed spectrum can be represented reasonably well by a simple power-law up to ~ 600 keV in the soft state (B. Philips 1997, private communication). A steeper power-law is required to fit the spectrum at low energies ($\lesssim 10$ keV), in addition to an ultra-soft component (Cui et al. 1997a; Dotani et al. 1997). The ultra-soft component is typical of BHCs (see review by Tanaka & Lewin 1995, and references therein), and is thought to be the emission from the innermost part of the accretion disk.

The observed spectral and temporal properties of Cyg X-1 both suggest that the hard X-rays are likely to be the product of inverse-Compton scattering of soft photons in the region by energetic electrons in a central corona surrounding the black hole (e.g., Ling et al. 1997; Cui et al. 1997c; Dove et al. 1997). Possible sources of the seed photons include emission from the accretion disk and synchrotron or bremsstrahlung emission near the black hole. The hard X-rays emerging from the corona may then illuminate the inner disk region, and the re-emitted photons from the disk could produce a so-called “Compton reflection bump” on the observed X-ray spectrum. This spectral feature has been observed for the hard state (Done et al. 1992; Ebisawa et al. 1996), but has not for the soft state, mostly due to the scarcity of high quality data.

Although ASCA observations are sensitive to soft spectral features and afford moderate energy resolution ($\Delta E/E \sim 8\%$ with GIS at the iron K-band), the limited energy range (0.7–10 keV) and a small effective area make ASCA insensitive to some spectral features such as broad and weak emission lines and/or absorption edges. On the other hand, RXTE observations cover a much wider energy range with a large effective area, but suffer from the converse problem

of lacking low-energy sensitivity below ~ 2 keV and energy resolution for studying narrow line emission. Therefore, the combination of the two instruments is powerful in disentangling various spectral components, thus provides more precise determination of the model parameters. In this letter, we present results from simultaneous ASCA and RXTE observations of Cyg X-1 near the end of its 1996 transition from the hard to soft state (Cui et al. 1997a).

2. Observations

Cyg X-1 was observed on 30 May 1996 by both *ASCA* and *RXTE* (Dotani et al. 1997; Cui et al. 1997a). The observations were scheduled independently, and fortuitously there was a ~ 1 ks overlap between them (UT 08:19:40 — 08:35:37). When the observations were made, the soft X-ray flux had already reached the soft-state level (Cui et al. 1997a), implying that the evolution of the accretion disk was perhaps completed. However, systematic studies of the spectral and timing properties during this period and comparison of the BATSE/CGRO and ASM/RXTE behavior during the ASM soft outburst suggest that the source had not settled down in the soft state yet, but very close (Cui et al. 1997a,b). The observed X-ray spectrum as well as the temporal properties varied during this transitional period (Cui et al. 1997a,b). It is therefore important to analyze the simultaneous data together, in order to compare results from two different instruments optimized for different energy ranges.

RXTE carries two co-aligned pointing instruments, the *Proportional Counter Array* (PCA; Jahoda et al. 1996) and the *High Energy X-ray Timing Experiment* (HEXTE). Due to the limited exposure time, the HEXTE data, which cover an energy range of 15-250 keV, suffer from poor statistics. Therefore, we only focus our attention on the PCA observation. The PCA has an effective area of about 6500 cm^2 . It covers a 2-60 keV energy range with moderate energy resolution ($\sim 18\%$ at 6 keV). ASCA also has two sets of detectors aboard, the *Gas Imaging Spectrometer* (GIS; Ohashi et al. 1996; Makishima et al. 1996) and the *Solid-state Imaging Spectrometer* (SIS; Burke et al. 1994). The SIS suffered from serious photon pile-up as well as severe telemetry saturation because Cyg X-1 was very bright during the observation (Dotani et al. 1997). Here we use only the GIS data.

3. Analysis and Results

The details on how the GIS data were reduced and the spectra extracted can be found in Dotani et al. (1997). For the PCA observation, the data from all five detectors are used here. The PCA background is now modeled, instead of using the earth-occultation data (Cui et al. 1997a), but the difference is negligible. To account for calibration uncertainties, we added 1% systematic error to the energy spectra for both the PCA and GIS. We simultaneously fitted the individual spectra for five detectors in the PCA (with response matrices version 2.1.2) and two

GIS spectra (with response matrices version 4.0 and XRT responses version 2.0 for ancillary response files; In addition, the default “ARF filter” was applied; cf. Fukazawa et al. 1997). The relative normalization between the GIS and PCA was allowed to vary due to the uncertainty in the PCA effective area with respect to that of GIS. The normalization parameters in the model are then determined with the GIS spectra.

First, we tried to find a simple analytic model which can adequately describe the observed spectra. Previous studies had shown that an ultra-soft component dominates the spectrum at low energies (Cui et al. 1997a; Dotani et al. 1997). We modeled this component with a multi-color disk model (MCD; Mitsuda et al. 1984; Makishima et al. 1986). The addition of a simple power law failed to reproduce the spectrum at high energies. A reasonable fit was instead obtained with a broken power-law with a very gradual high-energy cutoff. However, a careful examination of the PCA residual revealed a line feature at 6–7 keV. We added a broad Gaussian component to mimic the emission line, and indeed the fit was significantly improved. Table 1 summarizes the results of fits with and without the line. Note that the spectral flattening above ~ 10 keV is characteristic of Compton reflection.

Next, we refitted the spectrum with physical models available, to systematically study the effects of inverse Comptonization and Compton reflection on the X-ray spectrum. We experimented with MCD for the soft component and a Comptonized blackbody model by Nishimura et al. (1986) for the hard component (“compbb” hereafter). In the compbb model, free parameters are temperature and normalization of the blackbody component (for seed photons), and electron temperature and optical depth of the hot plasma. The fit is decent (Case 1 in Table 2), but significant residuals are apparent, as shown in Figure 1, in the 3–25 keV band where the PCA calibration uncertainty is small ($\lesssim 2\%$ for the total response, except for near the Xenon edge at ~ 4.8 keV; K. Jahoda 1997, internal memo, currently available at <http://lheawww.gsfc.nasa.gov/users/keith/pcarmfv2.1.2/pcarmfv2.1.2.html>). Inclusion or omission of the data above 25 keV hardly affects the model parameters ($< 3\%$). We added a Gaussian component to account for the line at ~ 6.6 keV. The broad “bump” peaked at ~ 15 keV is perhaps due to reflection, so we added a disk reflection component, based on a model by Magdziarz & Zdziarski (1995) (XSPEC model “pexriv”) which assumes a cutoff power law for the illuminating spectrum. Since the “compbb” spectrum with parameters appropriate for Cyg X-1 can be approximated by a cutoff power law with a photon index ~ 2.0 and cutoff energy ~ 100 keV, we used the “pexriv” model to calculate *only* the reflected spectrum with these parameters fixed in the fit. We also assume that the disk temperature is 10^5 K and its inclination angle 30° (same as in Done et al. 1992 and Ebisawa et al. 1996), and the gas in the disk is of solar abundances. The only remaining free parameters are the normalization (=solid angle Ω) and ionization parameter ξ . The residuals are now much reduced. Figure 2 shows the observed X-ray spectrum and the model (Case 2 in Table 2) with each component plotted separately. The results imply the presence of a highly ionized disk ($\xi > 12000$), in contrast to the hard state when $\xi \lesssim 100$ (Done et al. 1992; Ebisawa et al. 1996).

The emission line is found to be strong (with an equivalent width $EW \simeq 126$ eV) and broad. We also explored the presence of a weak narrow line, similar to that observed in the hard state (Done et al. 1992; Marshall et al. 1993; Ebisawa et al. 1996). We fixed the line width to zero, and the flux to $\sim 1.0 \times 10^{-3}$ photons $cm^{-2} s^{-1}$ (i.e., $EW \simeq 13$ eV, similar to that found in the hard state; Ebisawa et al. 1996). The fit is clearly worse (comparing Case 3 to Case 2 in Table 2), so the possibility of a weak narrow line is ruled out. To better characterize the intrinsic line width, however, we now focus only on the ASCA data, taking advantage of its superior energy resolution (~ 0.5 keV FWHM at 6.6 keV). We fixed the continuum parameters as well as the line energy to the best-fit values. The fit favors a strong broad line of width $E_\sigma = 0.6$ keV and EW 182 eV. Fixing EW at this value and the line width at 30 eV (much smaller than the instrument resolution; cf. Ebisawa et al. 1996) resulted in a larger χ^2 with the F-value, $(\Delta\chi^2/2)/(\chi^2/598) = 6.6$, thus such a line is ruled out at a confidence level of greater than 99.9%. If EW is allowed to vary, the fit results in a weaker ($EW \simeq 80$ eV) narrow line, but the χ^2 is still large, with the F-value 4.1; this can again be rejected at the ($>$)95% confidence level. We therefore conclude the iron emission line is broad in the soft state. It is also clear that the line energy is higher than in the hard state, which is consistent with a higher ionization state of the disk.

Dotani et al. (1997) derived a black hole mass of $12 \pm_1^3 M_\odot$, based on the ASCA data alone, applying the general relativistic accretion disk (GRAD) model by Hanawa (1989) for the soft component. They assumed the hard component to be a simple power-law with an iron absorption edge, since ASCA data alone is unable to constrain the hard component spectral shape precisely. To investigate how the mass estimation is affected by the inclusion of the RXTE data and different modeling of the hard component, we replaced the MCD model with the GRAD model in Case 2 and refitted the data. The inferred black hole mass is now $12.3_{-0.3}^{+0.5} M_\odot$, in excellent agreement with the ASCA measurement.

4. Discussion

As shown in Tables 1 and 2, the ultra-soft component is not very insensitive to the choice of models for the high-energy continuum: the temperature is in the range 0.39-0.44 keV, and the radius of the emitting region 72-93 km. The results confirm the fact that the temperature of the inner disk is higher in the soft state than in the hard state for Cyg X-1 (Ebisawa et al. 1996; Cui et al. 1997a; Dotani et al. 1997). This is consistent with the inner edge of the accretion disk being closer to the black hole in the soft state, because the bolometric X-ray luminosity changes little during the state transition (Zhang et al. 1997).

In addition to the ultra-soft component, the most probable model also requires a Comptonized hard component, a reflected component, and an emission line at ~ 6.6 keV. It should be noted that the Comptonized blackbody model we adopted does not take into account the high-energy spectral roll-over, so only applies to the energy range much below the cutoff energy at $\sim 3kT_e$. On the other hand, the observed electron temperature for the hot plasma is quite high, $kT_e \simeq 38$

keV, so the model is likely valid over the entire RXTE energy range. In any case, the Compton y -parameter ($= (4kT_e/mc^2)\tau$) should be relatively independent of various assumptions we made; the best-fit value is 0.28. It is interesting to point out that the measured temperature of Compton seed photons is significantly higher than that of the ultra-soft component and the radius of the emitting region is smaller. These seem to suggest that the seed photons are mostly from a region even closer to the black hole. However, this interpretation should be taken with caution, because the results depend on the choice of models for seed photons.

The results also show that the reflecting medium is highly ionized and its subtended solid angle is small ($\sim 0.15 \times 2\pi$). In fact, Fe XXV is the most abundant ion ($\sim 46\%$), then Fe XXVI ($\sim 35\%$) and Fe XXIV ($\sim 11\%$), based on the best-fit parameters. This ionization state is much higher than in the hard state, again consistent with the picture that the optically thick disk is closer to the black hole in the soft state. The small solid angle implies a geometry of a central corona surrounding the black hole and the reflection occurring mostly in the innermost portion of the disk where gas is highly ionized.

A broad iron emission line was observed at 6.58 ± 0.04 keV with an equivalent width ~ 126 eV. The fluorescent yields for Fe XXV, Fe XXVI, and Fe XXIV are 0.5, 0.7, and 0.75, respectively, which are much larger than that for neutral iron (0.34; Krolik & Kallman 1987). The weighted-average line energy taking account of the ion population and the fluorescent yield is therefore ~ 6.8 keV. The lower observed line energy and its broadness can perhaps be attributed to gravitational redshift and Doppler effects which become important if the emission line originates in the inner region of the disk. A similar line was also detected in GX 339-4, as well as an absorption edge at ~ 8.8 keV (Makishima et al 1986), so such features might be common to BHCs in the soft state. In comparison, the iron line observed in the hard state is centered at ~ 6.4 keV (Done et al. 1992; Marshall et al 1993; Ebisawa et al. 1996), so is likely due to cold iron. This is consistent with the inner disk edge being farther away thus cooler in the hard state. The line is broader and stronger in the soft state, even though the solid angle subtended by the reflecting medium is smaller. This is perhaps due to the combination of higher fluorescence yield for highly ionized iron and smaller photoelectric absorption of the ionized medium (cf. Krolik & Kallman 1987; Matt et al. 1993; Zycki & Czerny 1994).

We would like to thank S. N. Zhang for many useful discussions, and also Piotr Zycki on Compton reflection models. WC acknowledges support from NASA through Contract NAS5-30612.

REFERENCES

- Burke, B. E., Mountain, R. W., Daniels, P. J., Cooper, M. J., & Dolat, V. S. 1994, *IEEE trans. nucl. sci.* 41, 375
- Belloni, T., Méndez, M., van der Klis, M., Hasinger, G., Lewin, W. H. G., & van Paradijs, J. 1996, *ApJ*, 472, L107
- Cui, W. 1996, *IAU Circ.* 6404
- Cui, W., Heindl, W. A., Rothschild, R. E., Zhang, S. N., Jahoda, K., & Focke, W. 1997a, *ApJ*, 474, L57
- Cui, W., Zhang, S. N., Heindl, W. A., Rothschild, R. E., Jahoda, K., Focke, W., & Swank, J. H. 1997b, *Proceedings of 2nd Integral workshop "The Transparent Universe"*, Eds: C. Winkler et al. (St. Malo, France), *ESA-SP 382*, 209 (astro-ph/9610072)
- Cui, W., Zhang, S. N., Focke, W., and Swank, J. H. 1997c, *ApJ*, 484, 383
- Done, C., Mulchaey, J. S., Mushotzky, R. F., & Arnaud, K. A. 1992, *ApJ*, 395, 275
- Dotani, T., et al. 1997, *ApJ*, 485, L87
- Dove, J. B., Wilms, J., Maisack, M. & Begelman, M. C. 1997, *ApJ*, 487, 759
- Ebisawa, K., Ueda, Y., Inoue, H., Tanaka, Y., & White, N. E. 1996, *ApJ*, 467, 419
- Hanawa, T. 1989, *ApJ*, 341, 948
- Jahoda, K., et al. 1996, *EUV, X-ray, and Gamma-ray Instrumentation for Astronomy VII*, O. H. W. Siegmund and M. A. Gummin, eds., *SPIE 2808*, p. 59
- Krolik, J. H., & Kallman, T. R. 1987, *ApJ*, 320, L5
- Ling, J., et al. 1997, *ApJ*, 484, 475
- Marshall, F. E., Mushotzky, R. F., Petre, R., & Serlemitsos, P. J. 1993, *ApJ*, 419, 301
- Magdziarz, P., & Zdziarski, A. 1995, *MNRAS*, 273, 837
- Makishima, K. et al. 1986, *ApJ*, 308, 635
- Makishima, K. et al. 1996, *PASJ*, 48, 171
- Matt, G., Fabian, A. C., & Ross, R. R. 1993, *MNRAS*, 262, 179
- Mitsuda, K., et al. 1984, *PASJ*, 36, 741
- Nishimura, J., Mitsuda, K., & Itoh, M. 1986, *PASJ*, 38, 819

Ogawara, Y., et al. 1982, *Nature*, 295, 675

Ohashi, T. et al. 1996, *PASJ*, 48, 157

Tanaka, Y., & Lewin, W. H. G. 1995, in “X-ray Binaries”, eds. W. H. G. Lewin, J. van Paradijs, & E. P. J. van den Heuvel (Cambridge U. Press, Cambridge) p. 126

Zhang, S. N., Cui, W., Harmon, B. A., Paciesas, W. S., Remillard, R. E., & van Paradijs, J. 1997, *ApJ*, 477, L95

Zycki, P. T., & Czerny, B. 1994, *MNRAS*, 266, 653

Table 1. ^aFits to a Model of MCD,^bBroken Power-law with a High Energy Cutoff,^c and Line^d

N_H^e	T_{in} (keV)	R_{in} (km)	E_c (keV)	E_σ (keV)	N_l	α_1	E_b (keV)	α_2	N_p	E_c (keV)	E_f (keV)	χ^2_ν
$0.53^{+0.01}_{-0.02}$	$0.379^{+0.007}_{-0.004}$	101^{+3}_{-6}	$2.56^{+0.01}_{-0.02}$	$10.9^{+0.1}_{-0.1}$	$1.41^{+0.03}_{-0.05}$	$10.4^{+0.2}_{-0.4}$	$6.7^{+0.1}_{-0.2}$	38^{+2}_{-4}	1.8
$0.52^{+0.02}_{-0.01}$	$0.386^{+0.006}_{-0.006}$	93^{+4}_{-5}	$6.56^{+0.04}_{-0.06}$	$0.57^{+0.07}_{-0.07}$	$1.5^{+0.1}_{-0.2}$	$2.66^{+0.01}_{-0.02}$	$10.7^{+0.1}_{-0.1}$	$1.85^{+0.02}_{-0.02}$	$11.6^{+0.3}_{-0.5}$	19^{+2}_{-2}	132^{+16}_{-19}	1.3

^aErrors shown represent 90% confidence interval.

^b T_{in} and R_{in} are the temperature and radius of the inner disk, respectively, assuming a distance of 2.5 kpc for Cyg X-1.

^c α_1 and α_2 are power-law photon indices, and E_b the break energy. E_c is the cutoff energy, and E_f the e-folding energy. N_p is photon flux at 1 units of $photons\ cm^{-2}\ s^{-1}$.

^d E_c and E_σ are line energy and width, respectively, N_l photon flux in units of $10^{-2}\ photons\ cm^{-2}\ s^{-1}$.

^eHydrogen column density along the line of sight, in units of $10^{22}\ cm^{-2}$.

Table 2. ^aFits to a Model of MCD, Comptonized Blackbody^b Line, and Reflection^c

Case	N_H	T_{in} (keV)	R_{in} (km)	E_c (keV)	E_σ (keV)	N_l	T_b (keV)	T_e (keV)	τ	R_b (km)	$\Omega/2\pi$
1	$0.40^{+0.02}_{-0.01}$	$0.441^{+0.004}_{-0.003}$	78^{+3}_{-1}	$1.01^{+0.01}_{-0.01}$	$45.4^{+0.4}_{-0.7}$	$0.86^{+0.01}_{-0.01}$	$9.4^{+0.2}_{-0.1}$...
2	$0.40^{+0.01}_{-0.01}$	$0.436^{+0.004}_{-0.004}$	80^{+2}_{-1}	$6.58^{+0.05}_{-0.04}$	$0.35^{+0.07}_{-0.07}$	$1.0^{+0.1}_{-0.2}$	$0.90^{+0.02}_{-0.01}$	$38.7^{+0.3}_{-0.4}$	$0.93^{+0.01}_{-0.01}$	$11.8^{+0.1}_{-0.2}$	$0.15^{+0.03}_{-0.02}$
3	$0.39^{+0.01}_{-0.02}$	$0.450^{+0.006}_{-0.003}$	74^{+2}_{-2}	$6.6^{+0.1}_{-0.1}$	0 (fixed)	0.1 (fixed)	$1.00^{+0.03}_{-0.01}$	35^{+1}_{-1}	$0.89^{+0.01}_{-0.01}$	$9.3^{+0.1}_{-0.2}$	$0.40^{+0.05}_{-0.02}$

^aThe same as Table 1, unless otherwise noted.

^b T_b : blackbody temperature; T_e : electron temperature of the Comptonizing corona; τ : optical depth of the corona; and R_b is the radius of the region, assuming a distance of 2.5 kpc for Cyg X-1.

^c Ω is solid angle subtended by the reflecting medium, and ξ ionization parameter.

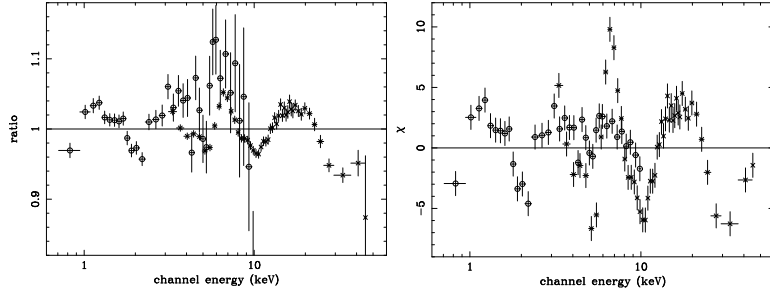


Fig. 1.— Residuals from a fit to the observed X-ray spectra with a model of MCD and compbb (Case 1 in Table 2). The left panel shows the data-to-model ratio, while the right one plots the value of χ to indicate the significance of deviations. The GIS data are represented by open circles, and the PCA data by asterisks. For display clarity, the spectra for two GIS detectors have been rebinned and coadded, so have those for five PCA detectors.

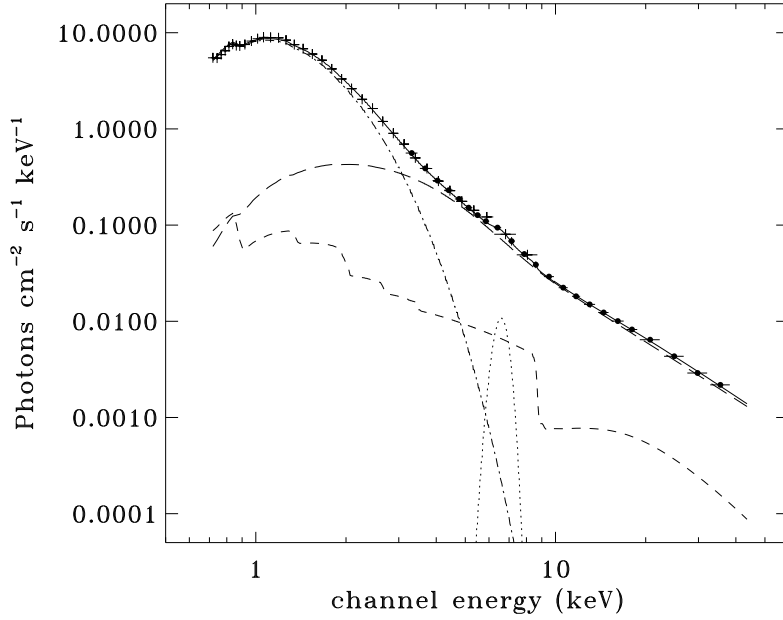


Fig. 2.— Observed GIS (in crosses) and PCA (in filled circles) spectra for Cyg X-1, along with the most probable model (Case 2 in Table 2) in solid line. The individual components are shown separately: MCD in dot-dashed line, compbb in long-dashed line, reflection component in short-dashed line, and Gaussian in dotted line. For display clarity, the spectra for two GIS detectors have been rebinned and coadded, so have those for five PCA detectors.